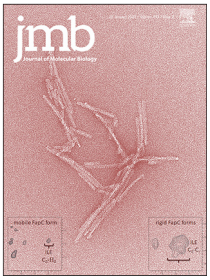

Architecture of the Tuberous Sclerosis Protein Complex

Kailash Ramlaul [1†], Wencheng Fu [2†], Hua Li [2†], Natàlia de Martin Garrido [1], Lin He [3], Manjari Trivedi [4], Wei Cui [4], Christopher H. S. Aylett [1*] and Geng Wu [2*]

*1 - **Section for Structural Biology,** Department of Infectious Disease, Imperial College London, Exhibition Road, London SW7 2BB, United Kingdom*
*2 - **State Key Laboratory of Microbial Metabolism,** School of Life Sciences & Biotechnology, The Joint International Research Laboratory of Metabolic & Developmental Sciences MOE, Shanghai Jiao Tong University, Shanghai, China*
*3 - **Instrumental Analysis Center,** Shanghai Jiao Tong University, Shanghai, China*
*4 - **Institute of Reproductive and Developmental Biology,** Department of Metabolism, Digestion and Reproduction, Imperial College London, Du Cane Road, London W12 0NN, United Kingdom*

***Correspondence to Christopher H.S. Aylett and Geng Wu:** c.aylett@imperial.ac.uk (C.H.S. Aylett), geng.wu@sjtu.edu.cn (G. Wu)*
https://doi.org/10.1016/j.jmb.2020.166743
Edited by Owen Pornillos

Abstract

The Tuberous Sclerosis Complex (TSC) protein complex (TSCC), comprising TSC1, TSC2, and TBC1D7, is widely recognised as a key integration hub for cell growth and intracellular stress signals upstream of the mammalian target of rapamycin complex 1 (mTORC1). The TSCC negatively regulates mTORC1 by acting as a GTPase-activating protein (GAP) towards the small GTPase Rheb. Both human TSC1 and TSC2 are important tumour suppressors, and mutations in them underlie the disease tuberous sclerosis. We used single-particle cryo-EM to reveal the organisation and architecture of the complete human TSCC. We show that TSCC forms an elongated scorpion-like structure, consisting of a central "body", with a "pincer" and a "tail" at the respective ends. The "body" is composed of a flexible TSC2 HEAT repeat dimer, along the surface of which runs the TSC1 coiled-coil backbone, breaking the symmetry of the dimer. Each end of the body is structurally distinct, representing the N- and C-termini of TSC1; a "pincer" is formed by the highly flexible N-terminal TSC1 core domains and a barbed "tail" makes up the TSC1 coiled-coil-TBC1D7 junction. The TSC2 GAP domain is found abutting the centre of the body on each side of the dimerisation interface, poised to bind a pair of Rheb molecules at a similar separation to the pair in activated mTORC1. Our architectural dissection reveals the mode of association and topology of the complex, casts light on the recruitment of Rheb to the TSCC, and also hints at functional higher order oligomerisation, which has previously been predicted to be important for Rheb-signalling suppression.

Introduction

Tuberous sclerosis complex (TSC) is an autosomal dominant disease characterised by benign tumours in multiple organs.[1] It is caused by mutations in either of the genes *TSC1* or *TSC2*, which encode the 130 kDa TSC1 and the 200 kDa TSC2 tumour suppressor proteins respectively. TSC1 contains an N-terminal α-helical 'core' domain and a coiled-coil at the C-terminus which is required for binding TSC2.[2–4] TSC2 contains a long α-solenoid domain at the N-terminus and a

C-terminal GTPase activating protein (GAP) domain, which is the sole catalytically active domain in the complex. Together with a small third subunit TBC1D7,[5] TSC1 and TSC2 assemble to form the TSC protein complex (TSCC).

TSCC signalling restricts cell growth by negatively regulating mTORC1, the central coordinator of metabolism.[6,7] Directly upstream of mTORC1, Rheb, a small GTPase localized to lysosomes through C-terminal farnesylation,[8] stimulates mTORC1 kinase activity when GTP-bound.[9] The TSCC stimulates Rheb GTPase activity, accumulating the GTPase in the inactive, GDP-bound, state to suppress mTORC1.[10] Spatial regulation of TSCC between the cytoplasm and lysosome is known to be pivotal for its function as a Rheb-GAP, with the current understanding being that the TSCC translocates to the lysosome surface to catalytically and sterically inhibit mTORC1 by binding to Rheb and sequestering it.[11,12] This translocation is reversed on TSC2 phosphorylation by AKT,[11] and other kinases, which are thought to regulate localisation through an unknown mechanism involving 14-3-3 binding,[13,14] as well as TSCC breakdown by ubiquitination-targeted TSC2 degradation.[15,16]

The architecture of the TSCC remains completely unknown, although small fragments of the complex have been structurally characterised. The core domain of *S. pombe* TSC1,[17] an N-terminal α-solenoid fragment of *C. thermophilum* TSC2,[18] and most recently the *Ct*TSC2$_{GAP}$ domain[19] have been resolved crystallographically. Furthermore, two co-crystal structures of TBC1D7 interacting with C-terminal coiled-coil fragments of TSC1 have been determined.[20,21] In this study, we have used cryogenic electron microscopy (cryo-EM) to examine the molecular architecture of the full-length, human holo-TSCC.

Results

We cloned human TSC1, TSC2, and TBC1D7 for expression in human embryonic kidney cells, and Rheb for expression in *Escherichia coli*. While both TBC1D7 and TSC1 could be expressed and purified independently, TSC2 could not be purified in the absence of TSC1 (Supp. Figure 1(A)), forming inclusions or being degraded in cell, consistent with the role of TSC1 in preventing TSC2 degradation.[15,16] We retrieved the complete human TSCC from lysate using FLAG-tagging, and purified the TSCC from most remaining contaminants by size-exclusion chromatography (SEC) (Supp. Figure 1(B)). Full-length TSCC yielded a broad peak with an estimated mass of 5200 kDa on SEC, due to oligomerisation through inter-TSCC interactions (Supp. Figure 1(C)). A clone yielding an internal deletion of TSC1(Δ400-600) was generated (Supp. Figure 1(D)) to minimise inter-complex interactions[2,23] for SEC-MALLS, yielding a defined peak with an estimated molecular weight by multi-angle LASER light scattering of 700 kDa (Supp. Figure 1(E)), roughly corresponding to a composition of 2:2:1-TSC1:TSC2:TBC1D7. Both full length and TSC1(Δ400-600) TSCC exhibited physiological GAP activity towards Rheb (Supp. Figure 1(F)).

We initially investigated the molecular architecture of the TSCC by negative staining (Supp. Figure 2). We observed extremely flexible, independent particles, however three defined ordered regions could be isolated, and two-dimensional averaging of these regions provided a complete picture (Figure 1(A)). The TSCC was extraordinarily elongated (~400 Å) and exhibited a characteristic "scorpion" shape, with a bulkier central "body", flexible "pincer"-like appendage at one end, and a barbed "tail" at the other. Cryo-EM of TSCC at low concentrations revealed identical particles (Supp. Figure 3(A) and (B)), whereas at higher concentrations we observed web-like networks which appear to be formed of head-to-tail TSCC particles (Supp. Figure 3(C)). Once again, complete TSCC particles were too flexible to average beyond low resolution. We isolated the same regions; both the "pincer" and "tail" proved to be strongly preferentially oriented and flexible, refining only to low-intermediate resolution (8.1 Å and 8.2 Å respectively) (Figure 1(B), Supp. Figure 4, Table 1). Because of the preferred orientation of TSCC particles on the grid, it was not possible to define a reliable persistence length for the TSCC HEAT repeat, however it is clear that the tips are substantially more flexible than the more proximal regions as would be expected. Recentring from the position of the body to the barb entailed a ~7 Å root-mean-squared deviation, while recentring from the body to the pincer regularly placed the resulting centres beyond the radius of convergence (i.e. at least 30 Å error). The body of the TSCC exhibited pseudo-C2 symmetry, and was refined in C2 initially, before symmetry was relaxed for a final C1 structure at 4.6 Å (Figure 1(B), Supp. Figure 4, Table 1).

The resolution of the "body" was high enough to trace chains and identify all secondary structural elements, but too low to definitively assign sequence. The published structure of the TSC2 GAP domain[19] fitted unambiguously into density adjoining a central α-solenoid on each side of the origin of C2 pseudo-symmetry (Supp. Figure 5(A)). At the juncture of the two α-solenoids, we observed a dimerisation interface comprising two back-to-back β-sheets. The topology and function of this dimerisation domain is conserved from that of the N-terminal domain of the RapGAP fold[22] (Supp. Figure 5(B)), although a domain swap between the two TSC2 molecules cannot be ruled out as the regions of secondary structure are separated by hundreds of disordered residues (Supp. Figure 6), however the interface formed is not, as TSC2 dimerises through

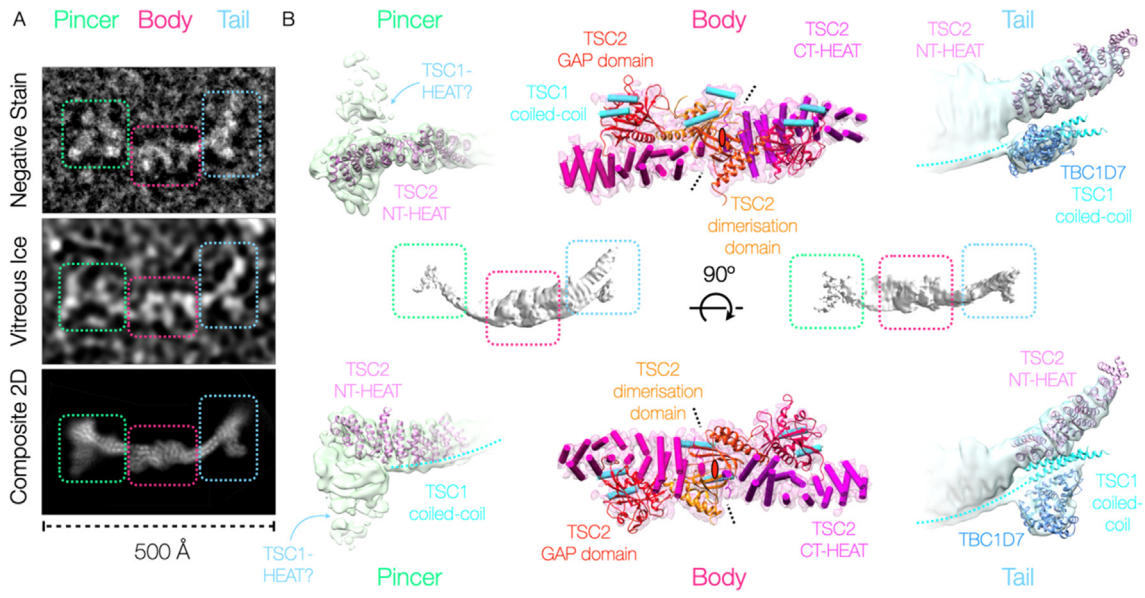

Figure 1. The TSC protein complex is an elongated, flexible, scorpion-like complex with a defined "pincer", "body", and barbed "tail". (A) Electron micrograph of a negatively stained TSCC particle on a carbon support, electron micrograph of a TSCC particle frozen within vitreous ice on a graphene oxide support, and composite 2D average image of the TSCC from the windowed regions of vitrified particles as indicated. The same regions, "pincer" (chartreuse), "body" (cerise), and "tail" (cerulean), are indicated through dashed boxes of the appropriate colour in both the representative particle image and the composite 2D class-average representation. (B) The overall structure of TSCC at low resolution (centre) and the refined densities corresponding to each region of the TSCC (indicated by boxes) are shown. In each case the reconstructed electron scattering density is shown as a transparent isosurface, while the corresponding fitted molecular structures (the TSC2 N-terminal HEAT-repeat,[18] the TBC1D7-TSC1 complex,[20,21] the TSC2-GAP domain,[19] and the RapGAP dimerisation domain[22]), and secondary structural elements in the case of the body, are shown in cartoon representation where available and practicable. The reconstructions have been rotated by 90° in the second panel as indicated.

back-to-back β-sheets instead of the end-on arrangement found in the case of RapGAP. With the exception of the GAP domain, the only β-elements remaining predicted within the sequence of any TSC protein are at the C-terminus of the α-solenoid of TSC2 (Supp. Figure 6), implying that the long disordered regions containing many of the phosphorylation sites regulating the TSCC are insertions within the C-terminal GAP domain. Our results are consistent with the TSC2 α-solenoids running outwards from C-terminus to N-terminus from the dimerisation site, and indeed there is a good fit of the TSC2 N-terminal HEAT repeat structure into the end of each of the "pincer" and "tail" (Figure 1 (B), Supp. Figure 5(C) and (D). The C2 symmetry of the TSC2 dimer is broken by two helices running directly across the top of the RapGAP-like dimerisation domain. This helical density forms a weakly connected "backbone" running over both GAP domains, and along the TSC2 α-solenoid outwards to both the "pincer" and "tail". We assign this continuous helical coiled-coil as that from the C-terminal regions of TSC1, implying that the two ends are its N- and C-terminus respectively. The "pincer" density is uninterpretable, however the density corresponding to the "barb" lying alongside the α-solenoid of the "tail" is completely separated from the remaining density, allowing it to be interpreted independently, and it unambiguously matches the TSC1-TBC1D7 structure[21] (Supp. Figure 5(D)). Under the reasonable assumption that this corresponds to its known binding site on the TSC1-coiled-coil we can therefore assign the orientation of the TSC1 dimer, implying that the "pincer" is made up of the TSC1 HEAT-domains.

Under the reasonable assumption that the GAP-Rheb interaction will mirror that of the published Rap-RapGAP complex,[22] we have docked Rheb accordingly (Supp. Figure 7(A)). The natural docking yields no clashes with the current structure, and implies a further interaction with the two helices adjoining the GAP domain which are conserved from the RapGAP fold (Figure 2(B)). We note that the Rheb farnesylation sites would both be situated on the same side of the TSCC, consistent with this being the correct orientation for lysosomal binding.

Discussion

We show that the TSCC forms an elongated, flexible architecture, comprising two copies of each of TSC1 and TSC2 and one of TBC1D7. The orientation of Rheb implied by the GAP domains (Figure 2(B)) matches the slight curvature of the complex, and the lysosomal membrane will therefore lie on the opposite side of the TSCC from the TSC1 backbone. While we were preparing this manuscript a study reporting the structure of a glutaraldehyde-crosslinked full-length TSCC has been Reference: https://www.researchsquare.com/article/rs-36453/v1? published as a preprint by Yang and colleagues. Their results are congruent with our own, although their structure is reported at higher resolution, allowing a full atomic model to be generated. The super-structure observed forming at higher concentrations (Supp. Figure 3(B)) may well play a part in retaining TSCC at the lysosome and reducing the off-rate once Rheb signalling has been suppressed as previously predicted.[11] Further structural investigation of these inter-TSCC interactions, likely mediated by the TSC1 termini,[2,23] is required to understand the higher-order organisation of TSCC and its role in mTORC1 regulation.

The RapGAP-like domain of TSC2 forms a dimer, as reported by Scrima and colleagues,[22] providing the centre of pseudosymmetry of the TSCC. The C2 symmetry of each of the dimeric TSC proteins is broken by the presence of the other, that of TSC1 by the curvature of its coiled-coil along the TSC2 α-solenoids, and that of TSC2 by the involvement of TSC1 in its dimerisation. We have confirmed once again that while TSC1 can fold independently of TSC2, the reverse does not occur.[15,16,24] Our architecture suggests a structural explanation for this observation; direct TSC1 involvement in the TSC2 dimerisation interface. The previously observed breakdown of TSC2, following ubiquitination in the absence of TSC1,[15,16] would be expected when structural elements cannot fold appropriately in the absence of their partner. This would also constrain the presence of functional TSC2 to subcellular regions containing TSC1 dimers.

TSC2 mutations are highly correlated with tuberous sclerosis. Half of these tumorigenic missense mutations occur within the N-terminal HEAT repeat (NTD) of TSC2 (27 of 54 residues in Supp. Table 1). Interestingly, most of these disease-targeting residues cluster together, such as A84/P91/E92, C244/M286/G294/E337/A357/R367, G440/L448/A460/R462/L466/L493, A583/H597/Y598/A607/R611/R622/M649, and L826/L847/R905/L916 (Supp. Figure 6). Given that the TSC2-NTD closely contacts the TSC2-GAP and TSC1-coiled coil in our structure, these clusters within the TSC2-NTD may represent the GAP- or TSC1-interacting surfaces. The TSC2-GAP domain possesses the second most tumorigenic missense mutations, with >30% of all sites (17 of 54 in Supp. Table 1). Many disease-related residues are highly conserved, such as H1620/G1642/N1643/R1743 (Supp. Figure 6). Residues H1620/G1642/N1643 in TSC2-GAP correspond to H266/G289/N290 of RapGAP, which directly contact or are very close to Rap in the Rap-RapGAP structure (Scrima *et al.*[22], Figure 2(A), Supp. Figure 7(B)). These residues are expected to interact with Rheb. In cancer cells harbouring these *TSC2* mutations, the TSC2-NTD/TSC2-GAP, or TSC1/TSC2, or TSC2-GAP/Rheb associations may be disrupted, leading to diminished GAP activity toward Rheb and abnormally elevated mTORC1 activity.

In our structure, the N-terminal part of TSC1 coiled coil is found to interact with the N-terminal HEAT domain of TSC2. Interestingly, this region of TSC1 is the highest conserved part among TSC1 homologues (Supp. Figure 8).

The Ras superfamily of GTPases comprise of five families: Ras, Rho, Ran, Rab, and Arf. The Ras family is further divided into six subfamilies: Ras, Rap, Rheb, Ral, Rad, and Rit. By comparing the sequences of Rheb homologues and other Ras family GTPases, we found three Rheb-specific

Table 1 Statistics of cryo-EM data collection and refinement for $TSCC_{FL}$.

$TSCC_{FL}$ data collection & processing			
	"Body" EMD-11819	"Pincer" EMD-11816	"Tail" EMD-11817
Magnification (×)	37,000	37,000	37,000
Voltage (kV)	300	300	300
Electron exposure (e^{-}/Å^2)	52.3 (first dataset) and 80.2 (second dataset)	52.3 (first dataset) and 80.2 (second dataset)	52.3 (first dataset) and 80.2 (second dataset)
Defocus range (μm)	0.75–3.25	0.75–3.25	0.75–3.25
Pixel size (Å/pix)	1.35	1.35	1.35
Symmetry imposed	C2, relaxed to C1 for final gold-standard refinement	C1	C1
Initial number of particles (no.)	1,306,527	1,306,527	1,306,527
Final number of particles (no.)	172,093	15,854	58,307
Map resolution (Å) at FSC = 0.143	4.6	8.1	8.2

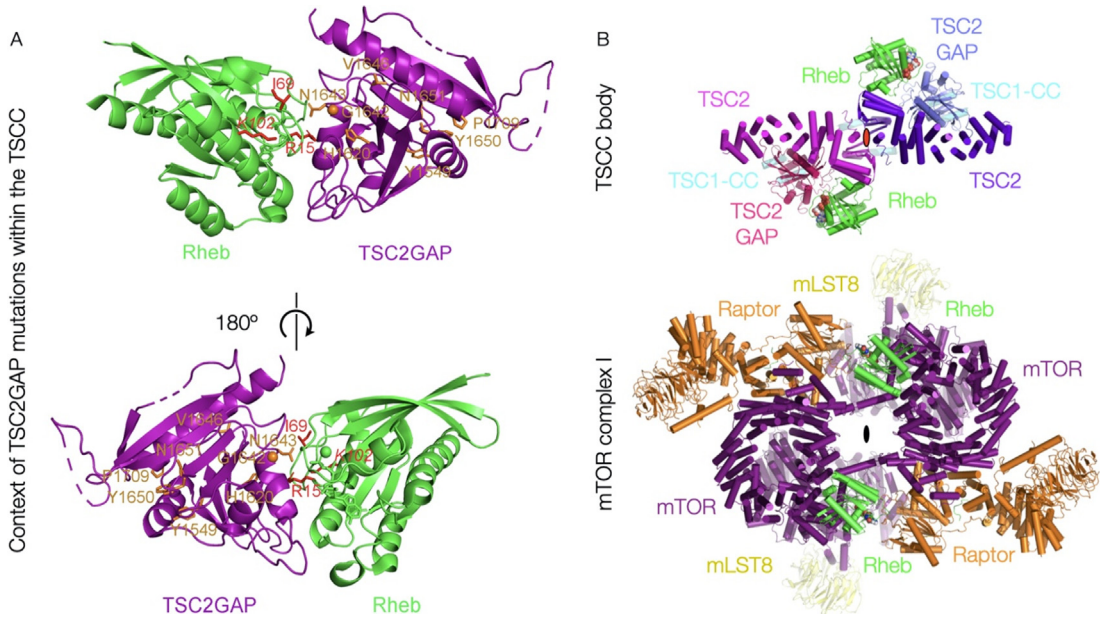

Figure 2. The TSCC central TSC2 GAP domains are poised to bind two Rheb molecules in interactions expected to be disrupted by key tumorigenic mutations. (A) A model of TSC2-GAP in complex with Rheb. The crystal structures of *Cf*TSC2$_{GAP}$ domain and human Rheb are superimposed onto the crystal structure of the RapGAP-Rap complex. *Cf*TSC2$_{GAP}$ residues corresponding to human TSC2 residues targeted by tumorigenic mutations in tuberous sclerosis are shown in stick representation and coloured in orange, labelled with human TSC2 residue numbers. The three Rheb residues identified to be conserved in Rheb homologues and Rheb-specific among Ras family GTPases are displayed in stick representation and coloured in red. The second panel has been rotated by 180° as indicated. (B) The docked fit of Rheb against the TSC2 GAP domain, based on the structure of the RapGAP-Rap1 complex, within the "body" of the TSCC, in comparison to its fit in the Rheb-activated structure of mTORC1. The secondary structural elements of the TSCC, and the molecular structure of mTORC1, are shown in cartoon representation.

residues: R15, I69, and K102, which are conserved in Rheb homologues but are different in all other Ras family, or subfamily, GTPases (Supp. Figure 9). Interestingly, these Rheb-unique residues all point toward TSC2-GAP in our model (Figure 2, Supp. Figure 7(B)) and GTPase assay data suggest that these residues are important for the TSC2-GAP interaction (Supp. Figure 7(C)).

In complete agreement with the conclusions of the Manning group,[11] the presence of the TSCC will both catalytically and sterically prevent Rheb–mTORC1 interactions during its GAP activity (Figure 2(B)), rotating the Rheb pair in relation to its position when interacting with mTORC1. The TSCC has been proposed to sequester GDP-Rheb after hydrolysis, which would be expected to occur at a different site from the GAP domains, and possibly with the TSCC in a different conformation due to association with the lysosomal membrane, as the catalytic complex will by its nature be transient. We believe that one of the more interesting observations from our results is that TSC2 binds Rheb as such a pair, as does mTORC1. Despite the fact that they are completely different in architecture and approach from different directions, the TSCC GAP domains are poised to bind two copies of Rheb at an almost identical separation to that resolved for Rheb in the structure of activated mTORC1 (Figure 2(B)). While it is possible that this is entirely happenstance, this would also be expected were Rheb bound by each partner as part of a greater, at least dimeric, complex on the lysosomal surface.

Our improved architectural understanding of the TSCC provides a starting point for the investigation of the molecular mechanisms by which TSCC directly regulates Rheb, and poses new questions on the nature of the superstructures formed by TSCC complexes, their partners, and the involvement of such quaternary structures in mTORC1 regulation.

Materials and Methods

Protein expression and purification

pRK7 plasmids subcloned with FLAG-tagged full-length (FL) human TSC1 (1164 amino acids, UniProtKB/Swiss-Prot accession number **Q92574-1**) and FLAG-tagged FL human TSC2 (1807 amino acids, UniProtKB/Swiss-Prot accession number **P49815-1**) were purchased from Addgene, and pRK7 was subcloned with FLAG-tagged human TBC1D7 (293 amino acids, GenBank accession number **AAH07054**). FL

TSC1-TSC2-TBC1D7 ($TSCC_{FL}$) plasmids, or TSC1 (Δ400-600)-TSC2-TBC1D7 ($TSCC_{1\Delta}$) plasmids, were co-transfected into human embryonic kidney (HEK) Expi293F cells (Thermo Fisher Scientific, Waltham, MA, USA). Two days after transfection, the harvested Expi293F cells were lysed by three cycles of freeze–thaw in lysis buffer (20 mM Tris, pH 8.0, 300 mM NaCl, 2 mM TCEP, 0.5 mM PMSF, 1 μg/ml aprotinin, and 1 μg/ml leupeptin), and TSCC was purified from the cell lysate by M2 anti-FLAG affinity chromatography (Sigma) followed by size exclusion chromatography using a Superose 6 column (GE Healthcare) pre-equilibrated with buffer containing 20 mM Tris, pH 8.0, 300 mM NaCl, and 2 mM TCEP. The identity of each TSCC component was verified by ESI-MS (Mass Spectrometry Facility, University of St. Andrews).

The cDNA residues 1–169 of human Rheb (184 amino acid isoform, GenBank accession number **EAW53989**) was subcloned into the pET28a vector (Novagen), with an N-terminal 6 × His-tag. Rhebwas overexpressed in *E.coli* strain BL21 (DE3). After lysis of the bacteria with a cell homogenizer (JNBIO) and clarification, the lysate was subjected to Ni^{2+}-NTA affinity chromatography (Qiagen) followed by size exclusion chromatography using a Superdex 200 column (GE Healthcare) pre-equilibrated with buffer containing 20 mM Tris, pH 8.0, 200 mM NaCl, and 2 mM DTT.

GTPase activity endpoint assay

The GTPase activity of Rheb was assayed using the QuantiChrom ATPase/GTPase assay kit (BioAssay Systems), in which the amount of released inorganic phosphate was measured through a chromogenic reaction with malachite green. In the assays 75 nM Rheb, either alone or mixed with 227.5 nM $TSCC_{FL}$, were added to the reaction buffer (40 mM Tris, pH 8.0, 80 mM NaCl, 8 mM magnesium acetate, 1 mM EDTA and 14 mM GTP) at 28 °C for 40 min. A further 200 μL of assay kit reagent was then added, and the reaction incubated for 20 min, before a microplate reading at OD 620 nm was measured. Spontaneous GTP hydrolysis was calculated by measuring background absorbance in the absence of Rheb and sample values were normalised by subtraction of background. Each experiment was repeated three times.

Size exclusion chromatography-multi-angle laser light scattering (SEC-MALLS)

$TSCC_{1\Delta}$ was analysed by SEC-MALLS using an Infinity liquid chromatography system (Agilent Technologies), linked to a Dawn Heleos multi-angle light scattering detector (Wyatt Technology) and Optilab T-rEX refractive index detector (Wyatt Technology). The sample was injected onto a Superose 6 10/300 size exclusion column (GE Healthcare) pre-equilibrated overnight with buffer containing 25 mM K-HEPES, pH 7.6, 250 mM KCl, 0.5 mM EDTA, 1 mM TCEP and trace amounts of NaN_3, using 0.2 mL/min flow rate at room temperature. In-line UV absorbance, light scattering and refractive index measurements were analysed using the ASTRA software package (Wyatt Technology) to determine molar mass estimates. The TSC1(Δ400–600) internal deletion construct was used for SEC-MALLS as prior studies have shown that this region contributes to higher-order oligomerisation or aggregation of the complex,[2,23] and therefore would confound attempts to derive a molecular weight estimate for the core complex.

Sample preparation for cryo-EM studies

$TSCC_{FL}$, after the above purification steps, was loaded onto a Superose 6 10/300 size exclusion chromatography column (GE Healthcare) pre-equilibrated with a preparation buffer containing 25 mM K•HEPES, pH 7.6, 175 mM KCl or 150 mM LiCl, 1 mM TCEP, and 0.5 μM EDTA. TSCC eluted as a single peak with a slight shoulder at lower retention volume. The integrity of the complex was confirmed by SDS-PAGE of both the peak and shoulder fractions. Main peak fractions were combined and concentrated to 0.1–0.2 mg/mL using Amicon 100 kDa molecular weight cut-off (MWCO) centrifugal filters and used for grid preparation.

Generation of an initial TSCC reference density

A sample of concentrated wild-type $TSCC_{FL}$ was applied to a carbon-coated holey carbon grid (R1.2/1.3, Quantifoil) and stained with 2% (w/v) uranyl acetate. A total of 224 micrographs were collected using an FEI Tecnai T12 electron microscope (Thermo Fisher Scientific, Waltham, MA, USA) at a magnification of 81,000-fold, an acceleration voltage of 120 kV, and a total dose of 50 $e^-/Å^2$ over a defocus range of −0.5 to −2.0 μm. A dataset of 9597 particles was selected manually using BOXER. The parameters of the contrast transfer function were determined using CTFFIND4. Particles were 2D-classified into 100 classes in two dimensions using RELION and sixteen well-defined classes were selected for initial three-dimensional reconstruction. Initial models were created using the initial model functions in EMAN2, refined in three dimensions at low resolution using SPIDER, then filtered to 60 Å and used as an initial reference for automatic refinement in RELION. The resulting initial model at a resolution of 26 Å, with independent volume Fourier Shell Correlation (FSC) of 0.143, was used for further refinement.

TSCC cryo-EM sample preparation

Samples of concentrated TSCC protein complexes were adsorbed to a thin film of graphene oxide deposited upon the surface of holey carbon copper grids (R2/1, 300 mesh, Quantifoil). Grids were blotted for 2–3 s before plunge freezing in liquid ethane using a Vitrobot Mark IV (Thermo Fisher Scientific, Waltham, MA, USA) at 4 °C and 100% humidity.

TSCC cryo-EM data collection

Data were collected of $TSCC_{FL}$ on a Titan Krios (Thermo Fisher Scientific, Waltham, MA, USA) at the Electron Bioimaging Centre (eBIC, Diamond Light Source), equipped with a K2 Summit direct electron detector (GATAN, San Diego, USA) and operated at 300 kV, 37,000-fold magnification and with an applied defocus range of −0.75 to −3.25 μm. Frames were recorded automatically using EPU, resulting in 5387 images of 3838 by 3710 pixels with a pixel size of 1.35 Å on the object scale. Images were recorded in two successive datasets (of 1880 and 3507 images, respectively) as either 40 or 60 separate frames in electron counting mode, comprising a total exposure of 52.3 or 80.2 $e^{-}Å^{-2}$, respectively. A separate dataset of $TSCC_{FL}$, which was not used for the determination of the final structure reported, was collected on a Titan Krios at the London Consortium for Cryo-EM (Francis Crick Institute, London, UK) equipped with a K3 direct electron detector (GATAN, San Diego, USA) and Volta phase plate. The microscope was operated at 300 kV and 81,000-fold magnification, with an applied defocus range of −1 to −3.25 μm. 4973 images were recorded, of 5760 by 4092 pixels, with a pixel size of 1.1 Å on the object scale.

TSCC cryo-EM data processing

Frames were aligned, summed and weighted by dose according to the method of Grant and Grigorieff using MotionCor2[25] to obtain a final image. Poor-quality micrographs were rejected based on diminished estimated maximum resolution on CTF estimation using CTFFIND4[26] and visually based on irregularity of the observed Thon rings. Particles were selected using BATCHBOXER,[27] and refinement thereafter performed using RELION3.[28,29]

Two-dimensional reference-free alignment was performed on ~1,500,000 initially boxed particles to exclude those that did not yield high-resolution class averages and to identify the principal ordered regions of the TSCC molecule. Of these, 395,622 particles populated classes extending to high-resolution and were retained for further refinement.

TSCC proved to be highly preferentially oriented on the grid, however it was possible to identify 2D classes for each of the “body”, “pincer” and “tail” regions. Iterated re-centring, two-dimensional refinement, and re-boxing using the neural network particle picker Topaz[30] was performed from the “body” region outwards in order to recover enough “pincer” and “tail” views to provide a complete description and definitive topology for all three regions.

Particles belonging to the “body” frequently displayed C2 symmetry in 2D class averages, and this particle subset was refined in three dimensions using this symmetry restraint. After several iterations of re-picking particles using Topaz[30] and refinement, the final gold-standard refinement of the “body”, including 172,093 particles, reached 4.2 Å at an independent FSC = 0.143. The symmetry was subsequently relaxed to C1 and refined (gold-standard) to 4.5 Å resolution at an independent FSC = 0.143. Reconstructions were also performed of the “pincer” and “tail” regions, from 15,854 and 58,307 particles respectively, however these suffered from persistent highly preferred orientation and conformational flexibility, with gold-standard refinements reaching 8.1 Å and 8.2 Å resolution, respectively, at an independent FSC = 0.143.

Architectural model of TSCC

The hand of the structure could be assigned from the maps based on the handedness of alpha-helices in the core of the body. We were also able to confirm the handedness of the density by determining the best possible fits of the known homologous structures into the density in either hand and then by local optimisation in Chimera. Maximal real-space CC values were 0.65 *versus* 0.58 for the GAP, and 0.55 *versus* 0.48 for the RapGAP dimerisation domain, into the correct hand *versus* the incorrect hand in each case. A poly-UNK secondary structural model of the TSCC “body” HEAT repeat sections and putative TSC1 coiled-coil helical sections was built using COOT.[31] The *C. thermophilum* TSC2-GAP structure (PDB ID: **6SSH**)[19] was unambiguously aligned with the region of density against each TSC2 HEAT repeat within the “body” using UCSF Chimera. The human RapGAP dimerisation domain crystal structure (PDB ID: **3BRW**)[22] was fit into the dimerisation interface between the two TSC2 HEAT repeats. In both the “pincer” and “tail” reconstructions, the *C. thermophilum* TSC2 N-terminal HEAT repeat crystal structure (PDB ID: **5HIU**)[18] could be fitted with the α-solenoid extending from C-terminus at the “body” dimerisation interface to N-terminus at either end of the elongated complex. Additionally, in the “tail” reconstruction the TBC1D7-TSC1 crystal structure (PDB ID: **5EJC**)[21] fit into density of the “barb”, providing a means to distinguish the “tail” from the “pincer”.

Data and Materials Availability

The cryo-EM density maps corresponding to the "pincer", "body", and "tail" of the *Hs*TSCC complex has been deposited in the EM Databank under accession codes **EMD-11816**, **EMD-11819**, and **EMD-11817**.

CRediT authorship contribution statement

Kailash Ramlaul: Investigation, Data curation, Writing - original draft, Writing - review & editing, Visualization. **Wencheng Fu:** Investigation, Writing - original draft, Writing - review & editing, Visualization. **Hua Li:** Investigation, Writing - review & editing. **Natàlia de Martin Garrido:** Investigation, Writing - review & editing. **Lin He:** Methodology, Resources, Writing - review & editing. **Manjari Trivedi:** Investigation, Writing - review & editing. **Wei Cui:** Resources, Writing - review & editing, Supervision. **Christopher H.S. Aylett:** Conceptualization, Methodology, Investigation, Resources, Data curation, Writing - original draft, Writing - review & editing, Visualization, Supervision, Project administration, Funding acquisition. **Geng Wu:** Conceptualization, Methodology, Investigation, Resources, Data curation, Writing - review & editing, Visualization, Supervision, Project administration, Funding acquisition.

Acknowledgements

The authors would like to thank Xinqiu Guo at Instrumental Analysis Centre of Shanghai Jiao Tong University for assistance with electron microscopy experiments. G.W. thanks Dr. Sheng Wang, Dr. Xinqi Gong, Lijun Yan, Hongpeng Wang, Ailiang He, and Dr. Yuan Gao for their contribution. We are indebted to the Imperial Centre for Structural Biology and the UK national electron Bio-imaging Centre at Diamond Light Source (proposal EM14769, funded by the Wellcome Trust, MRC and BBSRC) for access to electron microscopy equipment and in particular to Paul Simpson for technical support. The authors would also like to thank Marc Morgan for help with SEC-MALLS analysis, the St. Andrews Proteomics facility for mass spectrometric protein identification and Nadezhda Aleksandrova and Zining Zhu for performing biochemical assays.

G.W. is supported by the National Key R&D Program of China (YS2020YFA090044), National Natural Science Foundation of China (grant numbers 31670106 and 31872627), and Shanghai Jiao Tong University Scientific and Technological Innovation Fund. C.H.S.A. is supported by a Sir Henry Dale Fellowship jointly funded by the Wellcome Trust and the Royal Society (206212/Z/17/Z).

Author contributions

G.W. and C.H.S.A. conceived of the project. H.L., K.R., and W.F. purified the protein, performed initial negative staining analysis, and carried out the GAP assay. K.R. and N.M.G. carried out and analysed SEC-MALLS experiments. C.H.S.A., K.R., and W. F. prepared samples and grids for cryo-EM, collected electron micrographs and calculated single-particle reconstructions. All authors were involved in the interpretation of results and the drafting of the manuscript.

Declaration of Competing Interest

The authors declare that they have no competing financial interests.

Appendix A. Supplementary material

Supplementary data to this article can be found online at https://doi.org/10.1016/j.jmb.2020.166743.

Received 3 November 2020;
Accepted 2 December 2020;
Available online 8 December 2020

Keywords:
tuberous sclerosis complex;
hamartin;
tuberin;
cryo-EM;
RapGAP

† These authors contributed equally to this study.

References

1. Henske, E.P., Jóźwiak, S., Kingswood, J.C., Sampson, J. R., Thiele, E.A., (2016). Tuberous sclerosis complex. *Nature Rev. Dis. Prim.*, **2**, 16035. https://doi.org/10.1038/nrdp.2016.35.
2. Nellist, M., van Slegtenhorst, M.A., Goedbloed, M., Van den Ouweland, A.M., Halley, D.J., van der Sluijs, P., (1999). Characterization of the cytosolic tuberin-hamartin complex. Tuberin is a cytosolic chaperone for hamartin. *J. Biol. Chem.*, **274**, 35647–35652.
3. Santiago Lima, A.J., Hoogeveen-Westerveld, M., Nakashima, A., Maat-Kievit, A., Van Den Ouweland, A., Halley, D., Kikkawa, U., Nellist, M., (2014). Identification of regions critical for the integrity of the TSC1-TSC2-TBC1D7

complex. *PLoS One*, **9** https://doi.org/10.1371/journal.pone.0093940.
4. van Slegtenhorst, M., Nellist, M., Nagelkerken, B., Cheadle, J., Snell, R., van den Ouweland, A., Reuser, A., Sampson, J., et al., (1998). Interaction between hamartin and tuberin, the TSC1 and TSC2 gene products. *Hum. Mol. Genet.*, **7**, 1053–1057.
5. Dibble, C.C., Elis, W., Menon, S., Qin, W., Klekota, J., Asara, J.M., Finan, P.M., Kwiatkowski, D.J., et al., (2012). TBC1D7 is a third subunit of the TSC1}-{TSC2 complex upstream of {mTORC1}. *Mol. Cell.*, **47**, 535–546. https://doi.org/10.1016/j.molcel.2012.06.009.
6. González, A., Hall, M.N., (2017). Nutrient sensing and TOR signaling in yeast and mammals. *EMBO J.*, **36**, 397–408. https://doi.org/10.15252/embj.201696010.
7. Ramlaul, K., Aylett, C.H.S., (2018). Signal integration in the (m)TORC1 growth pathway. *Front. Biol. (Beijing)*,, 1–26. https://doi.org/10.1007/s11515-018-1501-7.
8. Clark, G.J., Kinch, M.S., Rogers-Graham, K., Sebti, S.M., Hamilton, A.D., Der, C.J., (1997). The Ras-related protein Rheb is farnesylated and antagonizes Ras signaling and transformation. *J. Biol. Chem.*, **272**, 10608–10615.
9. Yang, H., Jiang, X., Li, B., Yang, H.J., Miller, M., Yang, A., Dhar, A., Pavletich, N.P., (2017). Mechanisms of mTORC1 activation by RHEB and inhibition by PRAS40. *Nature*, **552**, 368–373. https://doi.org/10.1038/nature25023.
10. Huang, J., Manning, B.D., (2008). The TSC1}-{TSC2 complex: a molecular switchboard controlling cell growth. *Biochem. J.*, **412**, 179–190. https://doi.org/10.1042/{BJ20080281}.
11. Menon, S., Dibble, C.C., Talbott, G., Hoxhaj, G., Valvezan, A.J., Takahashi, H., Cantley, L.C., Manning, B.D., (2014). Spatial control of the TSC complex integrates insulin and nutrient regulation of mTORC1 at the lysosome. *Cell*, **156**, 771–785. https://doi.org/10.1016/j.cell.2013.11.049.
12. Demetriades, C., Plescher, M., Teleman, A.A., (2016). Lysosomal recruitment of TSC2 is a universal response to cellular stress. *Nature Commun.*, **7**, 10662. https://doi.org/10.1038/ncomms10662.
13. Shumway, S.D., Li, Y., Xiong, Y., (2003). 14–3-3β binds to and negatively regulates the tuberous sclerosis complex 2 ({TSC2}) tumor suppressor gene product, tuberin. *J. Biol. Chem.*, **278**, 2089–2092. https://doi.org/10.1074/jbc.C200499200.
14. Cai, S.-L., Tee, A.R., Short, J.D., Bergeron, J.M., Kim, J., Shen, J., Guo, R., Johnson, C.L., et al., (2006). Activity of TSC2 is inhibited by {AKT}-mediated phosphorylation and membrane partitioning. *J. Cell. Biol.*, **173**, 279–289. https://doi.org/10.1083/jcb.200507119.
15. Benvenuto, G., Li, S., Brown, S.J., Braverman, R., Vass, W.C., Cheadle, J.P., Halley, D.J., Sampson, J.R., et al., (2000). The tuberous sclerosis-1 (TSC1) gene product hamartin suppresses cell growth and augments the expression of the TSC2 product tuberin by inhibiting its ubiquitination. *Oncogene*, **19**, 6306–6316. https://doi.org/10.1038/sj.onc.1204009.
16. Chong-Kopera, H., Inoki, K., Li, Y., Zhu, T., Garcia-Gonzalo, F.R., Rosa, J.L., Guan, K.L., (2006). TSC1 stabilizes TSC2 by inhibiting the interaction between TSC2 and the HERC1 ubiquitin ligase. *J. Biol. Chem.*, **281**, 8313–8316. https://doi.org/10.1074/jbc.C500451200.
17. Sun, W., Zhu, Y.J., Wang, Z., Zhong, Q., Gao, F., Lou, J., Gong, W., Xu, W., (2013). Crystal structure of the yeast TSC1 core domain and implications for tuberous sclerosis pathological mutations. *Nature Commun.*, **4**, 2135. https://doi.org/10.1038/ncomms3135.
18. Zech, R., Kiontke, S., Mueller, U., Oeckinghaus, A., Kümmel, D., (2016). Structure of the Tuberous Sclerosis Complex 2 ({TSC2}) N terminus provides insight into complex assembly and tuberous sclerosis pathogenesis. *J. Biol. Chem.*, **291**, 20008–20020. https://doi.org/10.1074/jbc.M116.732446.
19. Hansmann, P., Brückner, A., Kiontke, S., Berkenfeld, B., Seebohm, G., Brouillard, P., Vikkula, M., Jansen, F.E., et al., (2020). Structural analysis of the TSC2 GAP domain: mechanistic insight into catalysis and pathogenic mutations in press *Structure*,. https://doi.org/10.1016/j.str.2020.05.008.
20. Gai, Z., Chu, W., Deng, W., Li, W., Li, H., He, A., Nellist, M., Wu, G., (2016). Structure of the TBC1D7}-{TSC1 complex reveals that TBC1D7 stabilizes dimerization of the TSC1 C-terminal coiled coil region. *J. Mol. Cell. Biol.*,. https://doi.org/10.1093/jmcb/mjw001.
21. Qin, J., Wang, Z., Hoogeveen-Westerveld, M., Shen, G., Gong, W., Nellist, M., Xu, W., (2016). Structural basis of the interaction between Tuberous Sclerosis Complex 1 ({TSC1}) and Tre2-Bub2-Cdc16 Domain Family Member 7 ({TBC1D7}). *J Biol Chem.*, **291**, 8591–8601. https://doi.org/10.1074/jbc.M115.701870.
22. Scrima, A., Thomas, C., Deaconescu, D., Wittinghofer, A., (2008). The Rap-{RapGAP} complex: GTP hydrolysis without catalytic glutamine and arginine residues. *EMBO J.*, **27**, 1145–1153. https://doi.org/10.1038/emboj.2008.30.
23. Hoogeveen-Westerveld, M., Exalto, C., Maat-Kievit, A., van den Ouweland, A., Halley, D., Nellist, M., (2010). Analysis of TSC1 truncations defines regions involved in TSC1 stability, aggregation and interaction. *Biochim. Biophys. Acta - Mol. Basis Dis.*, **1802**, 774–781. https://doi.org/10.1016/j.bbadis.2010.06.004.
24. Woodford, M.R., Sager, R.A., Marris, E., Dunn, D.M., Blanden, A.R., Murphy, R.L., Rensing, N., Shapiro, O., et al., (2017). Tumor suppressor Tsc1 is a new Hsp90 co-chaperone that facilitates folding of kinase and non-kinase clients. *EMBO J.*, **36**, https://doi.org/10.15252/embj.201796700 e201796700.
25. Zheng, S.Q., Palovcak, E., Armache, J.P., Verba, K.A., Cheng, Y., Agard, D.A., (2017). MotionCor2: Anisotropic correction of beam-induced motion for improved cryo-electron microscopy. *Nature Methods*, **14**, 331–332. https://doi.org/10.1038/nmeth.4193.
26. Rohou, A., Grigorieff, N., (2015). CTFFIND4: fast and accurate defocus estimation from electron micrographs. *J. Struct. Biol.*, **192**, 216–221. https://doi.org/10.1016/j.jsb.2015.08.008.
27. Tang, G., Peng, L., Baldwin, P.R., Mann, D.S., Jiang, W., Rees, I., Ludtke, S.J., (2007). EMAN2: an extensible image processing suite for electron microscopy. *J. Struct. Biol.*, **157**, 38–46. https://doi.org/10.1016/j.jsb.2006.05.009.
28. Scheres, S.H.W., (2012). RELION: Implementation of a Bayesian approach to cryo-EM structure determination. *J. Struct. Biol.*, **180**, 519–530. https://doi.org/10.1016/j.jsb.2012.09.006.
29. Zivanov, J., Nakane, T., Forsberg, B., Kimanius, D., Hagen, W.J., Lindahl, E., Scheres, S.H., (2018). RELION-3: new tools for automated high-resolution cryo-EM structure determination. *BioRxiv*, **7**, https://doi.org/10.1101/421123 421123.

30. Bepler, T., Morin, A., Noble, A.J., Brasch, J., Shapiro, L., Berger, B., (2018). Positive-unlabeled convolutional neural networks for particle picking in cryo-electron micrographs. *Nature Methods*, **10812**, 245–247. https://doi.org/10.1038/s41592-019-0575-8.

31. Emsley, P., Lohkamp, B., Scott, W.G., Cowtan, K., (2010). Features and development of Coot. *Acta Crystallogr. Sect. D Biol. Crystallogr.*, **66**, 486–501. https://doi.org/10.1107/S0907444910007493.